



Published in final edited form as:

FEBS J. 2015 May ; 282(10): 1922–1938. doi:10.1111/febs.13244.

## Insights into the slow-onset tight-binding inhibition of *Escherichia coli* Dihydrofolate Reductase: detailed mechanistic characterization of Pyrrolo [3,2-f] quinazoline-1,3-diamine and its derivatives as novel tight-binding inhibitors

Bharath Srinivasan<sup>a,b</sup> and Jeffrey Skolnick<sup>a,d</sup>

<sup>a</sup>Center for the Study of Systems Biology, School of Biology, Georgia Institute of Technology, 250, 14th Street, N.W., Atlanta, Georgia 30318, United States.

### Abstract

Dihydrofolate reductase, DHFR, is a pivotal enzyme involved in the *de novo* pathway for purine synthesis, and hence, represents an attractive target to disrupt systems that require rapid DNA turnover. The enzyme acquires resistance to available drugs by various molecular mechanisms, which necessitates the continuous discovery of novel antifolates. In a previous communication, we had identified a set of novel molecules that showed binding to *E. coli* DHFR by means of thermal shift without establishing whether they inhibited the enzyme. In this paper we show that a fraction of those molecules represent potent and novel inhibitors of DHFR activity. 7-[(4-aminophenyl)methyl]-7H-pyrrolo[3,2-f]quinazoline-1,3-diamine, AMPQD, a molecule with no reported inhibition of DHFR, potently inhibits the enzyme with a  $K_i$  value of  $7.42 \pm 0.92$  nM by competitive displacement of the substrate dihydrofolic acid. It shows uncompetitive inhibition vis-à-vis NADPH indicating that the inhibitor has markedly increased affinity for the NADPH-bound form of the enzyme. Further, we demonstrate that the mode of binding of the inhibitor to the enzyme-NADPH binary complex conforms to the slow-onset, tight-binding model. On the contrary, mechanistic characterization of the parent molecule 7H-pyrrolo[3,2-f] quinazoline-1,3-diamine, PQD, shows that the lack of (4-aminophenyl)-methyl group at the 7<sup>th</sup> position abolishes the slow-onset of inhibition. This finding provides novel insights on the role of substitutions on inhibitors of *E. coli* DHFR and represents the first detailed kinetic investigation of a novel daminopyrroloquinazoline derivative on a prokaryotic DHFR. Furthermore, marked differences in the potency of inhibition for the *E. coli* and human DHFR makes this molecule a promising candidate for development as an antibiotic.

### Keywords

Mechanistic characterization; dihydrofolate reductase; drug discovery; pyrrolo[3,2-f]quinazoline-1; 3-diamine; slow-tight-binding inhibition

<sup>b</sup>bharath.srinivasan@biology.gatech.edu. <sup>d</sup> Corresponding author, skolnick@gatech.edu, Tel: (404) 407-8975, Fax: (404) 385-7478.

#### Author Contributions

BS conceived of the study, participated in its design, carried out the experiments, analyzed and interpreted the results, and drafted the manuscript. JS conceived of the study, participated in its design and coordination, provided appropriate resources, helped analyze the data, and was involved in drafting and critically reviewing the manuscript. All authors read and approved the final manuscript.

## Introduction

Dihydrofolate reductase (E.C.1.5.1.3), DHFR, is a ubiquitous enzyme found in all kingdoms of life. The enzyme is involved in the reduction of 7,8-dihydrofolate (H<sub>2</sub>F) to 5,6,7,8-tetrahydrofolate (H<sub>4</sub>F) in which protonation of H<sub>2</sub>F on N5 precedes the hydride transfer from C4 of the NADPH cofactor to the C6 atom of the pterin ring on H<sub>2</sub>F [1]. Since DHFR is the sole source of cellular tetrahydrofolate, a metabolite essential for thymidylate and purine synthesis, its activity is indispensable. Thus, the enzyme represents an attractive target to disrupt systems that require rapid DNA turnover, e.g. proliferating cancer cells and pathogenic microbes[2]. *E. coli* DHFR has been extensively characterized in terms of kinetic mechanism, catalysis and structural studies[3-6]. This wealth of data makes the enzyme an attractive target to design small-molecule inhibitors as potential antibiotics. This has become all the more important given the rise in instances of nosocomial infection caused by drug-resistant *E. coli*[7]. However, designing inhibitors for DHFR presents considerable challenges since the enzyme acquires rapid resistance to available drugs by means of gene amplification, mutations and decreased drug uptake[8].

A lot of effort has been expended on discovering novel inhibitors for DHFR from different organisms given their potential applications to antineoplastic, anti-inflammatory and anti-infective drug discovery[9-11]. Methotrexate (MTX), a 2,4-diaminopteridin, is by far the most well characterized inhibitor for DHFR, showing a slightly increased potency of inhibition for parasitic DHFR compared to either human or bacterial DHFR [2]. Other prominent antifolates include the pyrimidine-2,4-diamines pyrimethamine, which is highly specific for eukaryotic DHFRs, trimethoprim (TMP), which shows a slightly greater preference for prokaryotic DHFRs[2], metoprine (DDMP) and piritrexim (PTX). Further, to overcome the limitation imposed by the hydrophilic nature of methotrexate, which hinders its distribution across different tissues, lipophilic inhibitors like trimetrexate (TMX), a quinazoline-2,4-diamine, have been synthesized as nonclassical inhibitors of DHFRs. Pyrrolo[3,2-f]quinazoline-1,3-diamine derivatives, containing a novel tricyclic heterocycle compared to TMX, were further explored and shown to be inhibitors of parasitic DHFRs[12]. Other studies have shown 7,8-dialkyl-1,3-diaminopyrrolo[3,2-f] quinazolines compounds as high-affinity inhibitors of DHFR from *Pneumocystis carinii* and *Candida albicans* [13]. In yet another study, a high throughput screen identified twelve compounds as inhibitors of *E. coli* DHFR[14]. However, it should be noted that detailed kinetic studies on the inhibition brought about by these novel DHFR inhibitors is lacking.

Previously, as part of experimental validation of the virtual ligand screening algorithm FINDSITE<sup>comb</sup> and relying on thermal shift assay methodology, we reported a set of novel molecules that showed binding to *E. coli* DHFR[15, 16]. In this paper, employing inhibition kinetics, we show that a fraction of those molecules represent novel inhibitors of DHFR activity and present detailed mechanistic characterization to substantiate our claims. By means of extensive steady-state and tight inhibition kinetics studies, for the first time we show that AMPQD and its parent compound, PQD, are novel tight-binding inhibitors of *E. coli* DHFR. These inhibitors preferentially bind to the NADPH-bound form of the enzyme at the H<sub>2</sub>F binding site. While AMPQD shows slow-onset of binding to the enzyme, PQD shows no such behavior implicating the (4-aminophenyl) methyl group as a possible origin

of slow-binding behavior in *E. coli* DHFR. This, combined with our already reported antibacterial, antifungal and antineoplastic activity by these compounds against two different strains of *E. coli* (multi-drug resistant *E. coli* and DH5 $\alpha$ ), a strain of methicillin resistant *Staphylococcus aureus*, a strain of vancomycin-resistant *Enterococcus faecalis*, a strain of amphotericin B resistant *C. albicans* and HCT-116 human colon carcinoma cell line, makes these compounds potential lead candidates to target conditions arising from aberrant DHFR activity. Further, pronounced differences in the potency of inhibition and the mode of inhibitor binding for AMPQD and PQD against *E. coli* and human DHFR makes these molecules attractive candidates for development as novel antibiotics.

## Results

### Inhibition of *E. coli* DHFR

All the hits from the FINDSITE<sup>comb</sup> experimental validation study were assessed for their ability to inhibit *E. coli* DHFR. The histogram in Fig 1 summarizes the results. All the reported inhibitors of DHFR from various sources *viz.*, methotrexate (NSC740), 7H-pyrrolo(3,2-f) quinazoline-1, 3-diamine (NSC339578), methylbenzoprim (NSC382035), pralatrexate (NSC754230), pemetrexed (NSC698037) and 6,7-bis (4-aminophenyl) pteridine-2, 4-diamine (NSC61642), show unambiguous inhibition of *E. coli* DHFR at a 1 mM inhibitor concentration. Prior to carrying out IC-50 determination and detailed inhibition studies, the kinetic parameters for the substrate H<sub>2</sub>F and cofactor NADPH were determined and found to be in agreement with values reported in the literature within experimental error [17, 18] (Table S1 and Fig S1). For all further experiments, except when a substrate is titrated, the substrates were kept at >10 times their respective  $K_m$  values. Table 1 and Fig S2A-B summarize the IC-50 values, defined as the concentration of inhibitor required to reduce the activity of the enzyme by 50%, determined for a select set of reported inhibitors of *E. coli* DHFR independently identified by our studies.

Among the nine novel binders reported by us in our previous study, seven were tested for their inhibition of *E. coli* DHFR[15]. Three (NSC309401, NSC80735 and NSC55152) showed almost complete inhibition while one molecule (NSC123458) showed approximately 87% inhibition at a 1mM inhibitor concentration (Fig 1). While NSC309401, AMPQD, is a substrate analogue with the quinazoline-1, 3-diamine group, NSC80735 and NSC55152 contain concatenated nitrophenyl and aminophenyl groups. To further understand their inhibition, IC-50 values were determined for the various molecules. Fig 2A shows the curve of log inhibitor concentration vs. activity for AMPQD giving an IC-50 value of  $189.0 \pm 1.0$  nM (Table 1). This number indicates potent inhibition comparable to that shown by methotrexate, with an IC-50 value of  $152.5 \pm 1.1$  nM. However, since it is known in the literature that IC-50 values are enzyme concentration dependent and can never get lower than  $[E_0]/2$  [19], it is highly likely that the number represents an underestimation of the actual affinity of the inhibitor for the enzyme (Fig 2B).

To account for this tight binding inhibition, the data were analyzed as per the methods developed by Morrison and coworkers[20, 21]. Fig 2C shows the fit of the data to the quadratic Morrison equation for tight binding and Table 1 lists the  $K_{iapp}$  values computed from non-linear curve fitting. As expected, the  $K_{iapp}$  value of  $7.8 \pm 0.8$  nM for AMPQD is

almost 25 fold lower than its IC-50. Further, compounds NSC80735, NSC55152 and NSC123458 were also titrated, and their log inhibitor concentration vs. activity were plotted to yield IC-50 values of  $36.56 \pm 1.1 \mu\text{M}$ ,  $176.5 \pm 1.1 \mu\text{M}$  and  $587.8 \pm 1.2 \mu\text{M}$ , respectively (Fig 2D and Table 1). However, since these three compounds are sparsely soluble in water, the reported IC-50 values may, at most, represent gross approximations. Moreover, their high IC-50s and relative insolubility may lead to potential problems of bioavailability. Hence, these compounds may not represent promising lead candidates. It is worthwhile to point out that compounds NSC80735 and NSC55152 didn't show either bactericidal activity or activity against cancer cells as reported in our previous study [15]. Detailed mechanistic characterization was undertaken on AMPQD (the best hit from the FINDSITE<sup>comb</sup> study), PQD (the parent molecule of AMPQD) and methotrexate (a well characterized DHFR inhibitor) to understand their mode of inhibition (Fig 3).

### **AMPQD (NSC309401) is a competitive inhibitor of dihydrofolate binding**

To further understand the inhibition shown by AMPQD, we resorted to detailed inhibition kinetics. Substrate dihydrofolate was titrated at several fixed concentrations of AMPQD, and the resulting curves from the primary plot, when globally fit to models for the various types of inhibition showed the best fit to the model for competitive inhibition (see Experimental Section for details) (Fig 4A) yielding a  $K_i$ , the equilibrium dissociation constant for the competitive inhibitor, of  $7.42 \pm 0.92 \text{ nM}$  (Table 2). Further, for visual assessment, the data were transformed and plotted as the double-reciprocal Lineweaver-Burk plot, LB. Fig 4B shows the lines of the LB-plot intersecting on the y-axis further indicative of competitive displacement of substrate dihydrofolate by AMPQD, whereby it increases the apparent  $K_m$  value for the substrate without unduly affecting the  $V_{max}$ . Further, this low  $K_i$  value, similar to that obtained from fit to the Morrison equation, reinforces the fact that AMPQD is a tight-binding inhibitor, a special case where the affinity of the inhibitor for the enzyme is an order-of-magnitude lower than the minimum concentration of enzyme that can be employed in the assay mix to get reliable activity. Further, the  $K_i$  value is ~25-fold lower than the obtained IC-50. However, the  $K_i$  value for AMPQD is approximately 2-fold higher than that reported for methotrexate (the reported value is ~ 3.6 nM[22]). The above data are conclusive about AMPQD binding to the same site as dihydrofolate and competing with the latter for high-affinity interactions with the enzyme. This competitive displacement can be ascribed to the quinazoline-1,3-diamine group shared by the two molecules (substrate and inhibitor) that might serve as the common motif responsible for binding. Though this behavior is similar to that shown by methotrexate, it is markedly different from that of a pyrimidine-2,4-diamine pyrimethamine against *Plasmodium* DHFR, which is a non-competitive inhibitor of the latter [23].

### **AMPQD (NSC309401) is an uncompetitive inhibitor of NADPH binding**

To understand AMPQD's effect on the cofactor NADPH binding, the latter was titrated at several fixed concentrations of AMPQD, and the resulting curves from the primary plot, when globally fit to models for the various types of inhibition showed the best fit to the model for uncompetitive inhibition (Fig 4C) yielding an  $\alpha K_i$ , the equilibrium dissociation constant for the uncompetitive inhibitor, of  $162.9 \pm 9.1 \text{ nM}$  (Table 2). This higher  $\alpha K_i$  value shows that AMPQD binding site is fully formed only when the enzyme is bound to NADPH.

It is worthwhile to point out that AMPQD  $K_i$  was  $\sim 7.4$  nM at saturating NADPH (see previous section). Further, for visual assessment, the resulting data were transformed and plotted as the double-reciprocal LB plot. Fig 4D shows parallel lines on the LB-plot confirming the fit of primary data to model for uncompetitive inhibition. The data on competition of AMPQD with NADPH is strongly indicative of an ordered binding event whereby NADPH binding facilitates inhibitor binding. It should be noted that this pattern of uncompetitive inhibition against NADPH is similar to the way MTX behaves (Fig S3A-B).

Though, in principle, *E. coli* DHFR can bind to both NADPH and H<sub>2</sub>F randomly as shown by some studies[6], productive catalysis proceeds through an ordered ternary complex formation with NADPH binding prior to dihydrofolate. Furthermore, the pattern is also consistent with the pH-independent and pH-dependent models for *E. coli* DHFR kinetic mechanism proposed by Fierke *et al* that shows that dihydrofolate always binds to the NADPH-bound form of the enzyme [4]. In a previous study, we have shown that AMPQD independently binds to the enzyme in the absence of NADPH. Hence, the type of inhibition should ideally be either noncompetitive or linear mixed-type. However, the difference between  $K_i$  and  $\alpha K_i$  is large. Hence, for all practical purposes, this inhibition can be considered as uncompetitive. Thermal shift assay measurements carried out from 0 nM - 500 nM AMPQD in the absence of NADPH were unsuccessful in stabilizing the protein and showed preferential binding to the denatured form of the protein. However, at a high concentration of 1mM, the inhibitor showed binding to the enzyme, even in the absence of added NADPH, as seen in the thermal stability profile (Fig S4). This further proves that AMPQD binding in the nM concentration range is absolutely conditional upon NADPH binding to the enzyme.

### 7H-Pyrrolo(3,2-f) quinazoline-1, 3-diamine (PQD) inhibition kinetics

PQD has been shown to possess inhibitory activity against DHFRs from eukaryotic sources, inhibiting fungal DHFRs [13]. In order to assess its inhibition of a prokaryotic enzyme, it was tested against *E. coli* DHFR (Fig 1 and Fig S2A). PQD is the parent molecule for AMPQD and lacking the latter's (4-aminophenyl) methyl group. Figs 5A-B show the primary curves for H<sub>2</sub>F titration at several different concentrations of PQD fit to the model of competitive inhibition and the double-reciprocal LB plot. Further, Fig 5C-D shows the primary curves for NADPH titration at several different concentrations of PQD fit to the model for uncompetitive inhibition and the double reciprocal LB plot. These patterns show that PQD occupies the H<sub>2</sub>F binding site and preferentially binds to the NADPH-bound form of the enzyme, mirroring the behavior shown by its derivative AMPQD. However, the  $K_i$  value of  $3.18 \pm 0.51$  nM for PQD is approximately half of that shown by AMPQD indicative of tighter binding (Table 2).

In an attempt to rationalize the ordered binding behavior, whereby all three inhibitors preferably bind to the NADPH-bound binary complex of the enzyme, structures of *E. coli* DHFRs in complex with NADPH (PDB ID: 1RX1) and methotrexate (PDB ID: 3DRC) were analyzed. When the structures were superimposed with their respective ligands, maximum change was noticed in the M20 loop that covers the active site where the hydride transfer reaction happens from NADPH to H<sub>2</sub>F (Fig 6A). Furthermore, it became clear that the

dramatic change in the orientation of M20 from the MTX-bound form to NADPH-bound form of the enzyme might be the principal reason of why the inhibitors prefer the NADPH-form (Fig 6A and 6B). This shift in the orientation between the two structures makes the thio group of methionine come within hydrogen bonding distance of the N8 group on MTX in the NADPH-bound structure. Since AMPQD shares this substructure with MTX, it is highly likely that this interaction with M20 increases the affinity of the inhibitor for the enzyme manifold. Further, apart from this principal interaction, the whole M20 loop with several charged and bulky residues undergoes a change between the two structures. Other residues that can have possible roles in this preferential binding of inhibitor to NADPH-bound form are M16 and E17.

### Slow onset tight binding inhibition: comparative study between AMPQD and PQD

AMPQD and PQD bind to *E. coli* DHFR with the same kinetic behavior as the well-characterized inhibitor methotrexate. Both are competitive with respect to H<sub>2</sub>F and show preferential binding to the NADPH-bound form. Since it is known that methotrexate shows a slow-onset tight binding mode to the enzyme[22], we wanted to ascertain whether this also holds true for AMPQD and PQD. The  $K_{iapp}$  values obtained for both AMPQD and PQD using steady state methods show that the inhibitors are tight-binding inhibitors (Table 1). Progress curve analysis was used to determine whether the inhibitors showed slow-onset of tight binding in inhibiting *E. coli* DHFR. Upon addition of AMPQD, the rate of product formation decreased exponentially with time from an initial velocity ( $v_i$ ) to a steady state velocity ( $v_s$ ) (Fig 7A). Additionally, both  $v_i$ ,  $v_s$  and the time required to reach  $v_s$  decreased with increasing concentrations of the inhibitor, whereas  $k_{obs}$  increased (Fig. 7A inset). This non-linear behavior in product formation in the presence of inhibitor complies with both the simple reversible slow-onset tight-binding inhibition model and inhibitor binding followed by isomerization model. However, upon assessing the effect of preincubation time with inhibitor on the steady state velocity of the reaction, whereby  $v/v_i$  was plotted against time at various fixed inhibitor concentrations, the behavior conformed to the classic reversible slow onset inhibition in which no isomerization happens after the rapid formation of the initial E-I complex (data not shown). A simple reversible equilibrium between the enzyme and inhibitor with association and dissociation rate constants  $k_3$  and  $k_{-3}$ , respectively, defines this model aptly as shown in Scheme I. This behavior is similar to that of any reversible inhibitor, except that the values of  $k_3$  and/or  $k_{-3}$  are smaller, leading to the slow-onset of inhibition. Further, as can be seen in the inset of Fig 7A, increase in  $k_{obs}$  is linear with respect to inhibitor concentration conforming to the mechanism of reversible slow binding with slope equal to  $k_3$  and y-intercept equal to  $k_{-3}$ . However, it should be noted that the measured value of  $k_3$  is apparent, since this rate constant is substrate concentration dependent as is seen in the  $v_i$  vs. AMPQD plot at several fixed concentrations of H<sub>2</sub>F (Fig 7B). Hence, the apparent value of  $K_i$  ( $K_{iapp}$ ) for an inhibitor of this type can be calculated from the ratio of  $k_{-3}/k_{3app}$ , which is equivalent to the ratio of the y-intercept/slope from the linear fit of the data plotted as in Fig 7A inset. The above analysis unequivocally proves that inhibition by AMPQD conforms to the classical slow-onset tight binding reversible inhibition.



When the time-dependent inhibition data for PQD was analyzed, it was clear that the inhibition can be merely classified as classical tight-binding reversible inhibition since the curves show no hint of biphasic non-linearity even at high concentration of the inhibitor (Fig 7C). Since PQD is the parent molecule of AMPQD, the slow onset behavior of the latter compound implicates the 4-aminophenyl methyl substitution at the 7<sup>th</sup> position. It should also be noted that, unlike the inhibition mode of PQD, AMPQD inhibition of the enzyme is similar to that shown by methotrexate (Fig 7D). However, the physical basis for the slow-onset behavior of both AMPQD and methotrexate in DHFRs remains unexplained, and we propose that substitutions on the 7H-Pyrrolo[3,2-f] quinazoline-1,3-diamine for AMPQD and 2,4-Diaminopteridin on MTX might be the principal determinant of the slow-onset behavior.

### Differential inhibition of human and *E. coli* DHFR

*E. coli* and human DHFR shares 28 % sequence identity and are structurally highly conserved (Fig S5). It is well demonstrated that inhibitors designed against prokaryotic DHFRs inhibit the activity of DHFRs from eukaryotic sources, given the high sequence and structural similarity of this protein across different evolutionary lineages[2]. There are several examples of such broad inhibition with the most prominent example being the commonly employed antifolate methotrexate, which is known to inhibit DHFRs from *E. coli*, rat and *Plasmodium* species [2]. However, differences in potency and mode of inhibition and the fact that antifolates target only rapidly proliferating cells like pathogenic microbes and tumors enables selective employment of them for specific treatment goals. With this aim, the hits obtained from the FINDSITE<sup>comb</sup> study[15] were assessed for their inhibitory activity on human DHFR. Fig 1 shows the comparative histogram of inhibition demonstrating that both human and *E. coli* DHFR are inhibited to similar extent at 1mM inhibitor concentrations. To understand the inhibition further, the IC-50 values for the various molecules were estimated (Table 1 , Fig 2A and Fig S2). Marked differences in the potency of AMPQD and PQD were seen in their inhibition of the homologous proteins from humans and *E. coli*. AMPQD, the novel hit from our study, showed an IC-50 of  $599.0 \pm 7.2$  nM for the human DHFR, which is about 3-fold less potent than the IC-50 for *E. coli* DHFR (Fig 2A and Table 1). The most dramatic difference was PQD's inhibition of human DHFR with an IC-50 value of  $3.09 \pm 0.17$   $\mu$ M, representing a 30-fold reduction in the potency of inhibition vis-à-vis *E. coli* DHFR (Fig S2A and Table 1). However, the IC-50 values for inhibition of human and *E. coli* DHFR by methotrexate were comparable, with a value of ~148 nM for the former and ~152 nM for the latter, respectively. For the rest of the molecules, the parameters are summarized in Table 1 and Fig S2B&C.

In order to further assess the effect of AMPQD on the human enzyme, competition experiments were performed by titrating H<sub>2</sub>F at several fixed concentration of AMPQD. The curves thus obtained were fit to various inhibition models with the best fit obtained for competitive inhibition (Fig 8A). Further, the double reciprocal LB plot shows intersection of the lines on the y-axis reinforcing the competitive inhibition (Fig 8B). This indicates that AMPQD inhibits the human enzyme by competitive displacement of substrate H<sub>2</sub>F, similar to its mode of action against the *E. coli* enzyme. However, the  $K_i$  value of  $22.47 \pm 3.66$  nM

for the human enzyme is almost 3-fold higher than that obtained for the *E. coli* enzyme (7.4 nM), indicative of poorer inhibition of the former.

Furthermore, upon analyzing the time-dependence of NADPH depletion in the presence of AMPQD for the human enzyme, no non-linearity was evident. This is indicative of neither slow onset nor slow dissociation of the inhibitor molecule to the human enzyme (Fig S6A). This is unlike the behavior displayed by the inhibitor AMPQD on the *E. coli* enzyme where prominent non-linearity was evident from the time-course of NADPH depletion in the presence of the inhibitor (Fig 7A). Likewise, PQD also didn't show any slow-onset of inhibition on the human enzyme exactly mirroring its behavior on *E. coli* DHFR (Fig S6B and 7B). The differences in the mode of inhibition by AMPQD of the human and *E. coli* enzyme is strongly indicative of differences in the binding site microenvironment between the two homologs. In fact, a recent study by Bhabha *et al*[24] has shown that despite high structural similarity, the dynamics of the active site loop movements varies substantially between human and *E. coli* DHFR. This, they hypothesize, results in markedly different inhibition by the product NADP<sup>+</sup> of the two homologs (IC-50 of ~620 μM for human DHFR versus ~5 mM for *E. coli* DHFR). However, inhibition of human DHFR by the known antifolate methotrexate shows signs of pronounced non-linearity in the time-course curves of NADPH consumption indicating that the inhibitor retains its slow-onset behavior as seen with *E. coli* DHFR (Fig S6C). Moreover, the plot of  $k_{\text{obs}}$  versus MTX concentration is hyperbolic, indicative of isomerization after inhibitor binding (Fig S6D). This is yet another behavior seen in the inhibition of the human enzyme that is markedly different from that shown for its *E. coli* counterpart whereby, in the case of the latter, there was no isomerization whatsoever as seen in the linear  $k_{\text{obs}}$  versus [MTX] plots (insets of Fig 7D).

## Discussion

Since DHFR is a pivotal enzyme in the synthesis of precursors of DNA, it has been the target for both anticancer and antibacterial drugs[2]. There has been a plethora of folate analogues that have been synthesized and tested for potential inhibitory activity against DHFRs from various sources[2, 25]. Principal among which are methotrexate, used prevalently as an anticancer drug, and trimethoprim, used as an antibacterial drug. In spite of multiple inhibitors designed against DHFRs from various organisms, detailed mechanistic characterization is available only for a few of these molecules. However, detailed kinetic characterization of an inhibitor is essential for designing efficient inhibitors with greater potency against the intended target, for determining the proper dose for testing on cellular/animal disease models and for understanding the pharmacodynamics. Further, since DHFR acquires rapid resistance to newly discovered antifolates, it is necessary to keep discovering novel small-molecules that inhibit this enzyme especially given the rise in instances of nosocomial *E. coli* infections in hospitalized patients. Several reports in literature highlight the fact that the incidence of *E. coli* mediated infections in hospitalized patients are on the rise, with one study showing multidrug resistant *E. coli* as the causative agent of UTI responsible for 40-50% of total nosocomial infections[7, 26-28]. Our study shows that AMPQD, a novel 7HPyrrolo[3,2-f]quinazoline-1, 3-diamine, is a potent inhibitor of the bacterial enzyme. Further, it also shows that compounds NSC80735, NSC55152 and NSC123458 show reasonable inhibition with μM IC-50 values and represent scaffolds



amenable to modifications for development of novel DHFR inhibitors. While NSC80735 and NSC55152 contain concatenated nitrophenyl and aminophenyl groups, NSC123458 is a dibenzazepine that is a common structural scaffold in many antidepressants and analgesics.

In the current study, detailed steady state inhibition experiments on *E. coli* DHFR have shown that the small-molecules AMPQD and PQD bind to the H<sub>2</sub>F binding site and prefer the NADPH-bound binary form of the enzyme. This hints at sequential binding of the substrates NADPH followed by H<sub>2</sub>F, given that the small-molecules are structural analogues of H<sub>2</sub>F. This order of substrate and substrate analogue binding is in conformity with those proposed in the literature[4]. Further, it is well documented in literature that NADPH exerts a synergistic effect on folate analogues binding to DHFR [29]. NADPH enhances the binding of all the classical (phenyltriazine, DADMP) and slow-binding (MTX, TMP) inhibitors of DHFR, while it has no effect on either pyrimethamine or folate binding to DHFR. It has been reported that the degree of NADPH synergism can vary as much as 1000 fold for the binding among the different folate analogues[29]. We posit that since NADP and NADPH are present in equal concentrations in the prokaryotic cytosol (as against the eukaryotic cytosol where NADP is no more than 1% of the concentration of NADPH)[30]), for an inhibitor to be an effective drug, it might be advantageous for it to inhibit the product-forming ternary form of enzyme. Hence, inhibitors showing greater synergy may be preferable as potential lead candidates.

Tight-binding inhibitors are an important class where the affinity of the inhibitor for its cognate enzyme is so high that the equilibrium assumptions employed to compute the affinity of the inhibitor for the enzyme no longer remain valid. Further, a lot of well-known inhibitors extensively employed as drugs also display the property of slow-onset of inhibition because of the time-dependent establishment of equilibrium between the enzyme-bound form and free inhibitor. A few examples are captopril[31], an angiotensin inhibitor, Dup697[32], a COX2 inhibitor, and methotrexate [22, 33], a DHFR inhibitor. Methotrexate inhibits DHFR in a time-dependent manner involving the rapid formation of enzyme-NADPH-MTX complex that undergoes relatively slow, reversible isomerization to form a thermodynamically stable ternary enzyme complex resulting in enhanced inhibition. Hence, the MTX concentration required for inhibition is comparable to the enzyme concentration employed in steady-state kinetic studies. This type of inhibition is categorized as slow-on/slow-off tight binding inhibition[22]. Other folate analogues that exhibit slow-onset, tight-binding inhibition are 5-deazamethotrexate, aminopterin and trimethoprim, though the extent to which they bring about isomerization for slow dissociation differs significantly. Here, we demonstrate that AMPQD shows a slow-onset tight-binding behavior similar to that shown by methotrexate. However, upon analyzing the time-dependent inhibition curves, it becomes obvious that there is no pronounced isomerization, if any, which could be detected. Mainly, the  $k_{obs}$  vs. inhibitor plots are linear both for AMPQD and MTX (Fig 7A and D) even at high inhibitor concentrations. Further, we could convincingly rule out the possibility that there is isomerization of the enzyme between two different forms with the inhibitor preferably binding to one form by the fact that  $k_{obs}$  increased (rather than decreased) with increasing inhibitor. For DHFR from *E. coli*, it has been reported that all folate analogues that act as tight binding inhibitors exhibit slow binding characteristics.

However slow-onset does occur without tight binding as observed with 5-deazafolate. To the best of our knowledge, for the first time, we show that PQD is a tight-binding inhibitor of DHFR not displaying any slow-binding behavior, as is evident from the linear time-course curves (Fig 7B).

Further, pronounced differences in the potency of inhibition of AMPQD and PQD for the human and *E. coli* homologue, with an order-of-magnitude higher affinity for the latter makes these molecules good candidates for development as effective antibiotics. It has been shown in the literature that recombinantly expressed human DHFR cannot complement DHFR-deficient *E. coli* cells, and this was ascribed to the differences in the dynamics and conformational plasticity of the active site loops across the two different DHFRs [24]. This conjecture is further validated by our studies showing similar site of binding on both human and *E. coli* DHFR for the inhibitor AMPQD ( $H_2F$  binding site) (see Fig 4A, Fig 8A) albeit with different modes (slow-onset tight binding for the *E. coli* enzyme, while merely tight-binding for the human homologue as in Fig 7A and Fig S6A). Further, the isomerization of MTX after initial binding on the human enzyme, as evident in the nonlinearity of  $k_{obs}$  versus MTX plot (Fig S6D), is completely absent from its binding to the *E. coli* DHFR (Fig 7D inset).

In conclusion, employing detailed inhibition kinetics, this study reports a set of novel and potent inhibitors of prokaryotic DHFR that have the potential to be developed as antibiotics for amelioration of conditions arising from bacterial infections. This, combined with the already reported antibacterial activity of AMPQD against two different strains of *E. coli* (Multi-drug resistant *E. coli* and DH5 $\alpha$ ), a strain of methicillin resistant *S. aureus* and a strain of vancomycin-resistant *E. faecalis*, makes this molecule a potential candidate for development as an antibiotic. Further, detailed kinetic assessment of the inhibition brought about by this molecule shows that it is competitive with respect to  $H_2F$  and uncompetitive with respect to NADPH, with a preference of the inhibitor molecule for the NADPH-bound form of the enzyme. Furthermore, we show that while AMPQD is a slow-onset tight binding inhibitor of *E. coli* DHFR, similar to methotrexate, PQD is merely a tight-binding inhibitor with no slow-onset behavior. This detailed kinetic characterization of the inhibitors, by means of providing additional insight on the structure-activity relationship, paves the way for development of better antifolates.

## Experimental Procedures

### Reagents

All reagents and chemicals, unless mentioned otherwise, were of high quality and were procured from Sigma-Aldrich Co., USA, Amresco, or Fisher Scientific. *E. coli* dihydrofolate reductase was provided by Prof. Eugene Shakhnovich, Harvard University. The small molecule 7-[(4-aminophenyl) methyl]-7H-Pyrrolo[3,2-f]quinazoline-1,3-diamine (NSC309401), methotrexate (NSC740), 7H-Pyrrolo(3,2-f) quinazoline-1, 3-diamine (NSC339578), methylbezoprim (NSC382035), pralatrexate (NSC754230), pemetrexed (NSC698037), 6,7-bis(4-aminophenyl) pteridine-2,4-diamine (NSC61642), 2,2'-iminostilbene (NSC123458), benzoylpas (NSC159686), cibaphthol RPH (NSC50690), NSC80735, NSC157522 and NSC55152 were provided by the Developmental Therapeutics

Program (DTP) of the National Cancer Institute (NCI), National Institutes of Health (NIH). Dihydrofolate reductase assay kit (CS0340) was obtained from Sigma (Sigma-Aldrich, St. Louis, MO) and contained 0.1 units of human DHFR (D6566), dihydrofolic acid, methotrexate and NADPH.

### Dihydrofolate reductase assay

The stock solutions of H<sub>2</sub>F and NADPH were reconstituted as per the manufacturer's instructions. DHFR catalyzes the transfer of a hydride from NADPH to H<sub>2</sub>F with an accompanying protonation to produce H<sub>4</sub>F. Overall, H<sub>2</sub>F is reduced to H<sub>4</sub>F and NADPH is oxidized to NADP<sup>+</sup>, resulting in a net decrease in the absorbance of NADPH at 340 nm. To understand the kinetics of *E. coli* DHFR and human DHFR, the rate of reduction of H<sub>2</sub>F to H<sub>4</sub>F was monitored by the decrease in absorbance at 340 nm for 100 seconds. The amount of product formed from the slope of initial velocity curves was computed using a molar extinction coefficient ( $\epsilon$ ) of  $6.2 \times 10^3 \text{ M}^{-1}\text{cm}^{-1}$  for  $\beta$ -NADPH at 340 nm [34]. The non-enzymatic hydrolysis of NADPH was normalized by monitoring the reaction in a double beam Hitachi U-2010 UV-Vis spectrophotometer (Hitachi High Technologies America, Inc., San Jose, CA, USA) with an appropriate blank. All the assays were carried out in the linear range of enzyme concentration. Assays were initiated with the addition of enzyme to the sample cuvette after zeroing the absorbance reading with respect to the reference cuvette. The initial velocities, where product formation was less than 5%, were measured for reaction mixtures containing 100 mM HEPES pH 7.3 at room temperature (~ 22 ° C).

To determine the  $K_m$  and  $V_{max}$  for H<sub>2</sub>F and NADPH, the respective substrate was titrated at fixed saturating concentration of the other, and the resultant velocities were plotted against substrate concentration and fit to equation 1 for one-site binding hyperbola

$$d[P]/dt = (V_{max} \times [S]) / (K_m + [S]) \quad (1)$$

where  $d[P]/dt$  is the rate of product formation,  $V_{max}$  is the maximum velocity,  $[S]$  is the substrate concentration and  $K_m$  is the Michaelis-Menten constant for the substrate assayed.

All the measurements were performed in duplicate, and the error values indicated are standard deviations (S.D.). The concentration of *E. coli* DHFR used was 16.7 nM (see below for protocol of enzyme concentration estimation). Unless mentioned otherwise, all the data were fit using non-linear curve fitting subroutines of GraphPad Prism, version 4.0 (GraphPad Software, Inc., San Diego, CA).

### Velocity-titration curves for enzyme concentration estimation

To interpret inhibition data without errors (see next section), an accurate estimate of catalytically active  $[E_t]$  is essential. Methods suggested in the paper by Williams *et al.*, 1979 [33], whereby velocity measurements after preincubation with a ligand (where enzyme-ligand complex is inactive and dissociates slowly) were followed to estimate the catalytically-active total enzyme concentration. Briefly, 0.1  $\mu\text{g}$  of *E. coli* DHFR and 0.16  $\mu\text{g}$  of human DHFR was preincubated with various concentrations of MTX in 100 mM HEPES pH 7.3 and 60  $\mu\text{M}$  NADPH for 300 seconds. The reaction was initiated with 50  $\mu\text{M}$  H<sub>2</sub>F, and the resultant velocity was plotted as a function of MTX concentration (Fig S7A-D). The

total concentration of the catalytically active enzyme is given by the intercept of the curve with the abscissa, which corresponds to 16.7 nM for of *E. coli* DHFR and 12.4 nM for human DHFR, respectively. The experiment was repeated with 600 seconds preincubation time giving identical results. The concentration was also estimated employing the molar extinction coefficient of 33460 M<sup>-1</sup> cm<sup>-1</sup> for the *E. coli* DHFR and 25440 M<sup>-1</sup> cm<sup>-1</sup> for human enzyme at 280 nm, respectively.

### Inhibition kinetics

Various inhibitors were assessed for their inhibitory effect on the dihydrofolic acid reducing ability of *E. coli* DHFR and human DHFR. Initial inhibition was assessed in a reaction mixture containing 100 mM HEPES pH 7.3, 60 μM NADPH, 50 μM H<sub>2</sub>F and 1 mM of each inhibitor. 16.7 nM of *E. coli* DHFR and 12.4 nM of human DHFR were used in the assay mix. Subsequently, both the potency of the inhibitor and its affinity for the enzyme were computed by experimental IC-50 determination and competition assays to determine its  $K_i$ . IC-50 determination assays were carried out in 100 mM HEPES pH 7.3, 60 μM NADPH, 50 μM H<sub>2</sub>F and variable concentration of each inhibitor. The enzyme concentration was as specified above. The curves were fit to equation (2), where I is the inhibitor concentration, and y is the percentage of activity.

$$y=100\% / [1 + (I/IC - 50)] \quad (2)$$

Furthermore,  $K_{iapp}$  were computed from the IC-50 curves by fitting them to the quadratic Morrison equation (3) for tight binding inhibition. This equation accounts for tight binding by doing away with the assumption that the free concentration of inhibitor equals the total concentration.

$$v_i/v_0=1 - \left( \left( [E]_T + [I]_T + K_i^{app} \right) - \sqrt{\left( [E]_T + [I]_T + K_i^{app} \right)^2 - 4[E]_T[I]_T} \right) / [E]_T \quad (3)$$

where  $v_i$  represents velocity in the presence of inhibitor,  $v_0$  represents velocity in the absence of inhibitor,  $[E]_T$  represents total enzyme,  $[I]_T$  represents total inhibitor and  $K_i^{app}$  represents apparent  $K_i$ .

Experimental  $K_i$  value determinations were carried out by titrating the substrates H<sub>2</sub>F and NADPH, around their respective  $K_m$  values, at various fixed concentrations of the inhibitors. The resulting [substrate] vs. velocity curves were fit to the models of competitive inhibition (equation 4), non-competitive inhibition (equation 5) and uncompetitive inhibition (equation 6) in order to discriminate between the different types of inhibition and to estimate the various inhibition constants ( $K_i$ ).

Competitive:

$$v=V_{max} [S] / \{K_m (1 + [I] / K_i) + [S]\} \quad (4)$$

Non-competitive:

$$v = V_{max} [S] / \{K_m (1 + [I] / K_i) + [S] (1 + [I] / K_i)\} \quad (5)$$

Uncompetitive:

$$v = V_{max} [S] / (K_m + [S] (1 + [I] / K_i)) \quad (6)$$

where  $v$  is the velocity of the reaction,  $V_{max}$  is the maximum velocity,  $[S]$  is the substrate concentration, and  $[I]$  is the inhibitor concentration.  $K_m$  is the Michaelis-Menten constant, and  $K_i$  is the inhibition constant. Visual assessment of the type of inhibition was undertaken by plotting the double reciprocal Lineweaver-Burk plot from experimental data points constituting the primary plot.

### Progress Curve Analysis: Slow tight binding

The slow-onset inhibition of *E. coli* and human DHFR brought about by AMPQD, PQD and MTX was monitored by initiating the reaction with 16.7 nM of *E. coli* DHFR and 12.4 nM of human DHFR in assay mixtures containing 100 mM HEPES pH 7.3, 50  $\mu$ M H<sub>2</sub>F, 60  $\mu$ M NADPH and varying concentration of inhibitor (0-25  $\mu$ M). The reactions were allowed to proceed until the progress curve became linear, indicating that the enzyme has attained steady state. To ensure that substrate depletion does not significantly affect the reaction rate, substrate concentrations greater than 10 times the respective  $K_m$  values were used. Progress curves were analyzed as described previously[35]. Briefly, the resulting progress curves were fit to the integrated rate Eq. 7 for slow binding inhibition by nonlinear regression analysis.

$$A_t = A_0 - v_s \times t - (v_i - v_s) (1 - \exp(-k_{obs} \times t)) / k_{obs} \quad (7)$$

Where,  $A_t$  and  $A_0$  are the absorbance at time  $t$  and time 0,  $k_{obs}$  is the pseudo-first order rate constant for approach to the steady state, whereas  $v_i$  and  $v_s$  correspond to the initial and final slopes of the progress curve. Values for  $v_i$ ,  $v_s$ , and  $k_{obs}$  were obtained at each inhibitor concentration. Progress curves were approximately linear in the absence of added inhibitor. The values of  $k_{obs}$ ,  $v_i$ , and  $v_s$  obtained from the fit to equation 7 were replotted to obtain the  $k_{off}$  and  $k_{on}$  for inhibitor binding for a classical single-step inhibition mechanism in which rapid reversible binding of the inhibitor occurs to the enzyme.

Further, the patterns were also analyzed for possible two-step inhibition mechanism. In this case, which signifies a second slow step of isomerization after inhibitor binding to form the final enzyme-inhibitor complex, the following equation was used to fit the replot of  $k_{obs}$  vs inhibitor to gauge its non-linearity.

$$k_{obs} = k_{-4} + k_4 [I] / (K^{-app}_{-1} + [I]) \quad (8)$$

where  $k_4$  and  $k_{-4}$  represent the forward and reverse rate constants for the isomerization step.

### Thermal shift assay methodology

High throughput thermal shift assays were carried out following established guidelines [36, 37]. Briefly, thermal melt curves for proteins were obtained from samples aliquoted in 96-

well plates using a RealPlex quantitative PCR instrument from Eppendorf (Eppendorf, NY, USA) with 5 X Sypro orange dye as the fluorescent probe (Invitrogen). ( $\lambda^{\text{excitation}}$  is 465 nm and  $\lambda^{\text{emission}}$  is 580 nm). A heating gradient of 1 °C/min from 25 °C to 75 °C was used. The thermal melt experiments were done in 100 mM HEPES pH 7.3 and 150 mM NaCl with 20  $\mu$ l total volume of the reaction mix. The concentration of AMPQD was varied from 0 nM-500 nM at 5  $\mu$ M of *E. coli* DHFR. All experiments were done in duplicate, with the mean value considered for further analysis.

The curves were fit to Boltzmann's equation (Eq. 9) for estimating the  $T_m$  (melting temperature) from the observed intensity of fluorescence,  $I$ .

$$I = I_{min} + \left( [I_{max} - I_{min}] / \left( 1 + e^{((T_m - T)/a)} \right) \right) \quad (9)$$

$I_{min}$  and  $I_{max}$  are the minimum and maximum intensities;  $a$  denotes the slope of the curve at the transition midpoint temperature,  $T_m$  [36]. Thermodynamic parameters were estimated as specified in the previous literature [15].

## Supplementary Material

Refer to Web version on PubMed Central for supplementary material.

## Acknowledgements

This project was funded by GM-37408 and GM-48835 of the Division of General Medical Sciences of the NIH. The authors wish to thank Prof. Eugene Shakhnovich, Harvard University, for providing purified *E. coli* DHFR protein. We would also like to thank the Developmental Therapeutics Program of the National Cancer Institute for providing the small molecules used in this study.

## Abbreviations

<b>DHFR</b>	dihydrofolate reductase
<b>AMPQD</b>	7-[(4-aminophenyl) methyl]-7H-pyrrolo[3,2-f] quinazoline-1, 3-diamine
<b>PQD</b>	7H-pyrrolo[3,2-f] quinazoline-1, 3-diamine
<b>NADPH</b>	nicotinamide adenine dinucleotide phosphate, reduced
<b>H<sub>2</sub>F</b>	dihydrofolate
<b>MTX</b>	methotrexate

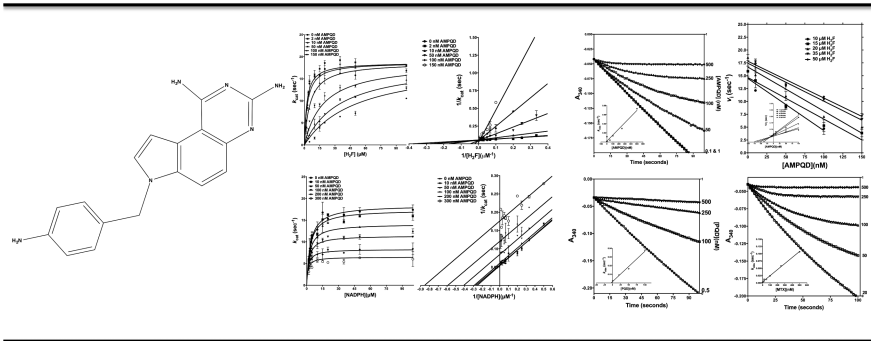
## References

1. Liu CT, Francis K, Layfield JP, Huang X, Hammes-Schiffer S, Kohen A, Benkovic SJ. Escherichia coli dihydrofolate reductase catalyzed proton and hydride transfers: Temporal order and the roles of Asp27 and Tyr100. Proceedings of the National Academy of Sciences of the United States of America. 2014; 111:18231–6. [PubMed: 25453098]
2. Schweitzer BI, Dicker AP, Bertino JR. Dihydrofolate reductase as a therapeutic target. FASEB journal : official publication of the Federation of American Societies for Experimental Biology. 1990; 4:2441–52. [PubMed: 2185970]

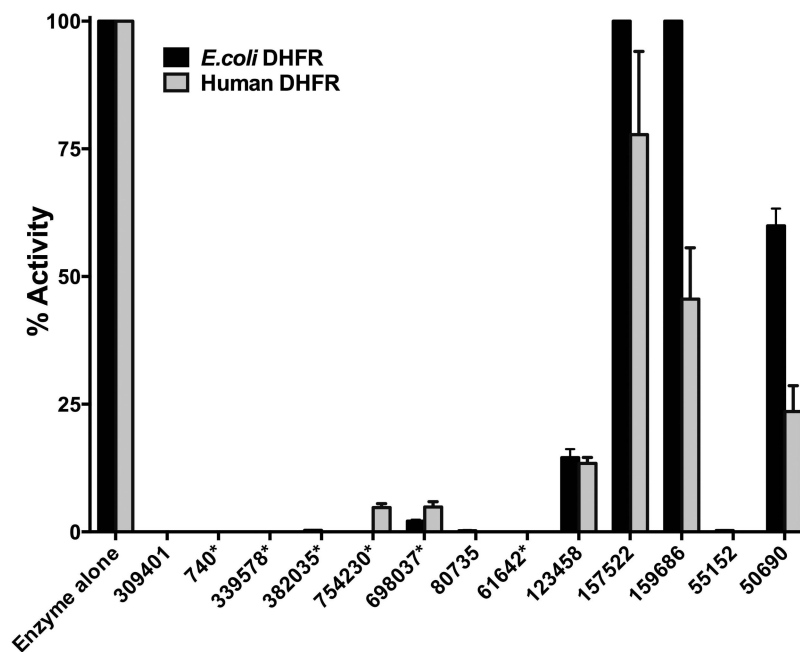


3. Sawaya MR, Kraut J. Loop and subdomain movements in the mechanism of Escherichia coli dihydrofolate reductase: crystallographic evidence. *Biochemistry*. 1997; 36:586–603. [PubMed: 9012674]
4. Fierke CA, Johnson KA, Benkovic SJ. Construction and evaluation of the kinetic scheme associated with dihydrofolate reductase from Escherichia coli. *Biochemistry*. 1987; 26:4085–92. [PubMed: 3307916]
5. Cayley PJ, Dunn SM, King RW. Kinetics of substrate, coenzyme, and inhibitor binding to Escherichia coli dihydrofolate reductase. *Biochemistry*. 1981; 20:874–9. [PubMed: 7011378]
6. Stone SR, Morrison JF. Kinetic mechanism of the reaction catalyzed by dihydrofolate reductase from Escherichia coli. *Biochemistry*. 1982; 21:3757–65. [PubMed: 6753919]
7. Bean DC, Krahe D, Wareham DW. Antimicrobial resistance in community and nosocomial Escherichia coli urinary tract isolates, London 2005–2006. *Annals of clinical microbiology and antimicrobials*. 2008; 7:13. [PubMed: 18564430]
8. Borst P, Ouellette M. New mechanisms of drug resistance in parasitic protozoa. *Annual review of microbiology*. 1995; 49:427–60.
9. Gonen N, Assaraf YG. Antifolates in cancer therapy: structure, activity and mechanisms of drug resistance. *Drug Resist Updat*. 2012; 15:183–210. [PubMed: 22921318]
10. Hagner N, Joerger M. Cancer chemotherapy: targeting folic acid synthesis. *Cancer Manag Res*. 2010; 2:293–301. [PubMed: 21301589]
11. Chio LC, Queener SF. Identification of highly potent and selective inhibitors of Toxoplasma gondii dihydrofolate reductase. *Antimicrob Agents Chemother*. 1993; 37:1914–23. [PubMed: 8239605]
12. Guan J, Zhang Q, O'Neil M, Obaldia N 3rd, Ager A, Gerena L, Lin AJ. Antimalarial activities of new pyrrolo[3,2-f]quinazoline-1,3-diamine derivatives. *Antimicrob Agents Chemother*. 2005; 49:4928–33. [PubMed: 16304154]
13. Kuyper LF, Baccanari DP, Jones ML, Hunter RN, Tansik RL, Joyner SS, Boytos CM, Rudolph SK, Knick V, Wilson HR, Caddell JM, Friedman HS, Comley JC, Stables JN. High-affinity inhibitors of dihydrofolate reductase: antimicrobial and anticancer activities of 7,8-dialkyl-1,3-diaminopyrrolo[3,2-f]quinazolines with small molecular size. *J Med Chem*. 1996; 39:892–903. [PubMed: 8632413]
14. Zolli-Juran M, Cechetto JD, Hartlen R, Daigle DM, Brown ED. High throughput screening identifies novel inhibitors of Escherichia coli dihydrofolate reductase that are competitive with dihydrofolate. *Bioorg Med Chem Lett*. 2003; 13:2493–6. [PubMed: 12852950]
15. Srinivasan B, Zhou H, Kubanek J, Skolnick J. Experimental validation of FINDSITE(comb) virtual ligand screening results for eight proteins yields novel nanomolar and micromolar binders. *J Cheminform*. 2014; 6:16. [PubMed: 24936211]
16. Srinivasan, B.; Skolnick, J.; Zhou, H. Molecules with potent DHFR binding affinity and antibacterial activity in (USPTO, ed). Georgia Tech Research Corporation; (Atlanta, GA, US), United States: 2014.
17. Murakami C, Ohmae E, Tate S, Gekko K, Nakasone K, Kato C. Cloning and characterization of dihydrofolate reductases from deep-sea bacteria. *Journal of biochemistry*. 2010; 147:591–9. [PubMed: 20040594]
18. Stone SR, Morrison JF. Dihydrofolate reductase from Escherichia coli: the kinetic mechanism with NADPH and reduced acetylpyridine adenine dinucleotide phosphate as substrates. *Biochemistry*. 1988; 27:5493–9. [PubMed: 3052577]
19. Cha S. Tight-binding inhibitors-I. Kinetic behavior. *Biochemical pharmacology*. 1975; 24:2177–85. [PubMed: 1212266]
20. Morrison JF. Kinetics of the reversible inhibition of enzyme-catalysed reactions by tight-binding inhibitors. *Biochimica et biophysica acta*. 1969; 185:269–86. [PubMed: 4980133]
21. Williams JW, Morrison JF. The kinetics of reversible tight-binding inhibition. *Methods in enzymology*. 1979; 63:437–67. [PubMed: 502865]
22. Stone SR, Montgomery JA, Morrison JF. Inhibition of dihydrofolate reductase from bacterial and vertebrate sources by folate, aminopterin, methotrexate and their 5-deaza analogues. *Biochemical pharmacology*. 1984; 33:175–9. [PubMed: 6367748]

23. Tahar R, de Pecoulas PE, Basco LK, Chiadmi M, Mazabraud A. Kinetic properties of dihydrofolate reductase from wild-type and mutant *Plasmodium vivax* expressed in *Escherichia coli*. *Molecular and biochemical parasitology*. 2001; 113:241–9. [PubMed: 11295178]
24. Bhabha G, Ekiert DC, Jennewein M, Zmasek CM, Tuttle LM, Kroon G, Dyson HJ, Godzik A, Wilson IA, Wright PE. Divergent evolution of protein conformational dynamics in dihydrofolate reductase. *Nature structural & molecular biology*. 2013; 20:1243–9.
25. Abraham A, McGuire JJ, Galivan J, Nimec Z, Kisliuk RL, Gaumont Y, Nair MG. Folate analogues. 34 Synthesis and antitumor activity of nonpolyglutamylatable inhibitors of dihydrofolate reductase. *Journal of medicinal chemistry*. 1991; 34:222–7. [PubMed: 1992121]
26. Schaberg DR, Culver DH, Gaynes RP. Major trends in the microbial etiology of nosocomial infection. *The American journal of medicine*. 1991; 91:72S–75S. [PubMed: 1928195]
27. Caini S, Hajdu A, Kurcz A, Borocz K. Hospital-acquired infections due to multidrug-resistant organisms in Hungary, 2005-2010. *Euro surveillance : bulletin Europeen sur les maladies transmissibles = European communicable disease bulletin*. 2013; 18
28. Hassan SA, Jamal SA, Kamal M. Occurrence of multidrug resistant and ESBL producing *E coli* causing urinary tract infections. *Journal of basic and applied sciences*. 2011; 7:39–43.
29. Stone SR, Morrison JF. Mechanism of inhibition of dihydrofolate reductases from bacterial and vertebrate sources by various classes of folate analogues. *Biochimica et biophysica acta*. 1986; 869:275–85. [PubMed: 3511964]
30. Appleman JR, Beard WA, Delcamp TJ, Prendergast NJ, Freisheim JH, Blakley RL. Unusual transient- and steady-state kinetic behavior is predicted by the kinetic scheme operational for recombinant human dihydrofolate reductase. *The Journal of biological chemistry*. 1990; 265:2740–8. [PubMed: 2303423]
31. Baudin B, Beneteau-Burnat B. Mixed-type inhibition of pulmonary angiotensin I-converting enzyme by captopril, enalaprilat and ramiprilat. *Journal of enzyme inhibition*. 1999; 14:447–56. [PubMed: 10536878]
32. Dannhardt G, Kiefer W. Cyclooxygenase inhibitors--current status and future prospects. *European journal of medicinal chemistry*. 2001; 36:109–26. [PubMed: 11311743]
33. Williams JW, Morrison JF, Duggleby RG. Methotrexate, a highaffinity pseudosubstrate of dihydrofolate reductase. *Biochemistry*. 1979; 18:2567–73. [PubMed: 36135]
34. Horecker BL, Kornberg A. The extinction coefficients of the reduced band of pyridine nucleotides. *The Journal of biological chemistry*. 1948; 175:385–90. [PubMed: 18873313]
35. Rawat R, Whitty A, Tonge PJ. The isoniazid-NAD adduct is a slow, tight-binding inhibitor of InhA, the *Mycobacterium tuberculosis* enoyl reductase: adduct affinity and drug resistance. *Proceedings of the National Academy of Sciences of the United States of America*. 2003; 100:13881–6. [PubMed: 14623976]
36. Niesen FH, Berglund H, Vedadi M. The use of differential scanning fluorimetry to detect ligand interactions that promote protein stability. *Nature protocols*. 2007; 2:2212–21.
37. Crowther GJ, He P, Rodenbough PP, Thomas AP, Kovzun KV, Leibly DJ, Bhandari J, Castaneda LJ, Hol WG, Gelb MH, Napuli AJ, Van Voorhis WC. Use of thermal melt curves to assess the quality of enzyme preparations. *Analytical biochemistry*. 2010; 399:268–75. [PubMed: 20018159]

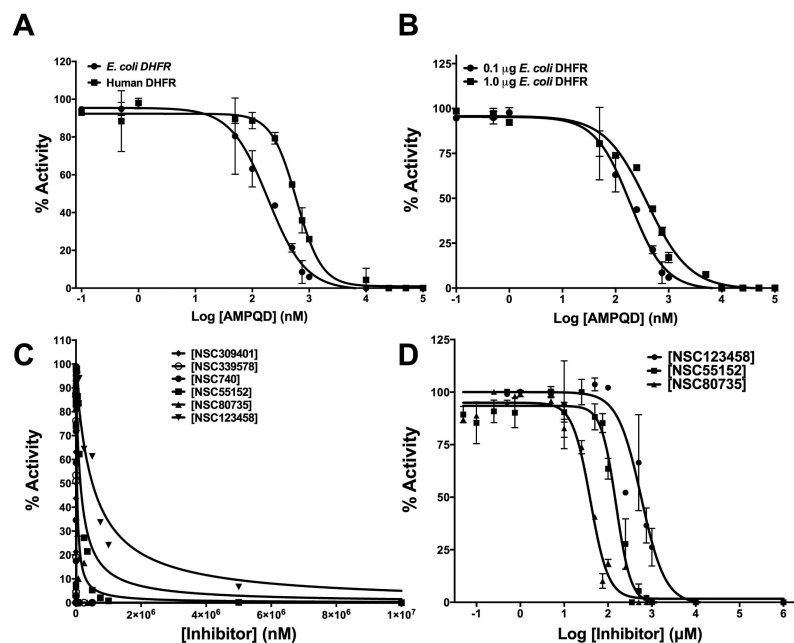


SCHEME I.



**Fig 1.**

Comparative inhibition of DHFR from *E. coli* and humans. Each histogram represents the activity of *E. coli* (black histograms) or human DHFR (gray histograms) in the presence of the inhibitor molecules tested at a fixed concentration of 1 mM. All activities are expressed as percentage activity with respect to the enzyme control for ease of comparison across the two enzymes. The numbered notations for the various inhibitor molecules represent NSC numbers. The numbers with an asterisk represent molecules that have been previously reported as having DHFR inhibitory activity from various organisms and independently “predicted” by our method.

**Fig 2.**

Potency of inhibition. (A) IC-50 determination for AMPQD against *E. coli* and human DHFR. (B) Enzyme concentration dependence of IC-50 for the tight-binding inhibitor AMPQD for *E. coli* DHFR. (C) Fit of the experimental dose-response curves to Morrison's equation for tight-binding for inhibitors of *E. coli* DHFR. (D) IC-50 value estimates for inhibitors of *E. coli* DHFR not displaying tight-binding behavior (NSC80735, NSC55152 and NSC123458). On the plots, the y-axis represents % activity of the enzyme and the x-axis represents the log inhibitor concentration/inhibitor concentration. The experimental data points were fit to the respective equations using the non-linear curve-fitting algorithm of GraphPad Prism v 6.0e.

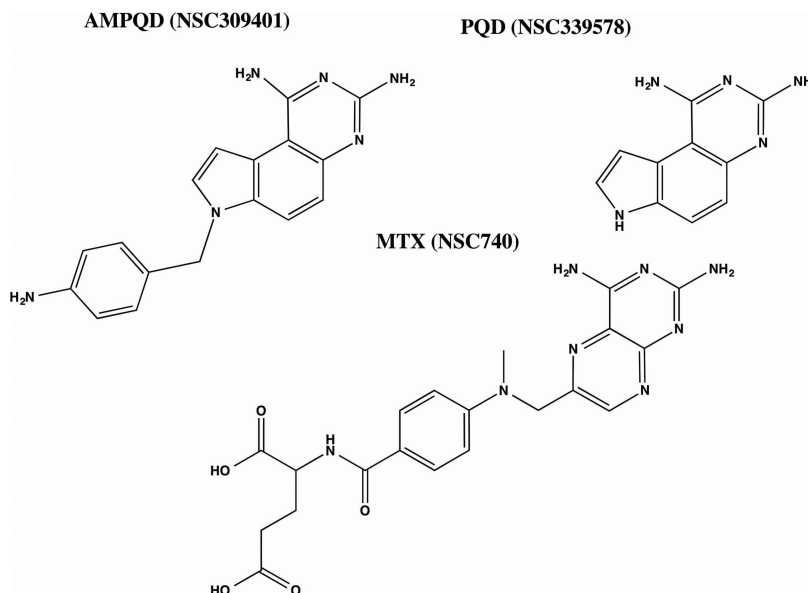


**Fig 3.** Structures of (A) AMPQD (NSC309401) (B) PQD (NSC339578) and (C) MTX (NSC740). The SDF files for the structures were downloaded from PubChem database and the figures were made in ChemBioDraw 14.0.



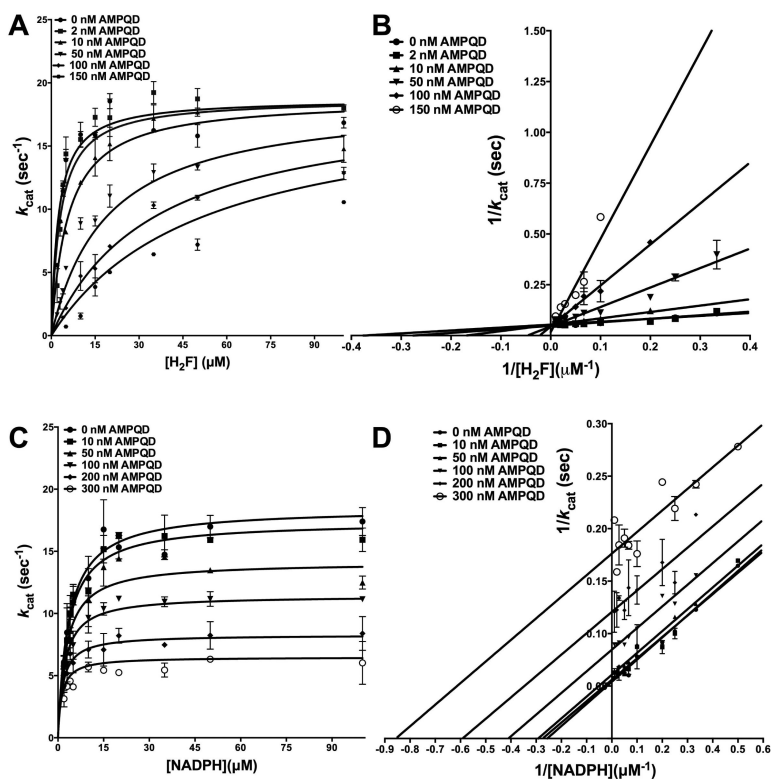


**Fig 4.** Inhibition kinetics of AMPQD (NSC309401) for *E. coli* DHFR (A) Fit of the primary data to the competitive inhibition model for H<sub>2</sub>F titration at several fixed concentrations of AMPQD. (B) Double reciprocal Lineweaver-Burk plot of H<sub>2</sub>F titration at several fixed concentrations of AMPQD. (C) Fit of the primary data to the uncompetitive inhibition model for NADPH titration at several fixed concentrations of AMPQD (D) Double reciprocal Lineweaver-Burk plot of NADPH titration at several fixed concentrations of AMPQD. The y-axis shows the  $k_{\text{cat}}$  value. The experimental data points were fit to the respective models using the non-linear curve-fitting algorithm of GraphPad Prism v 6.0e.

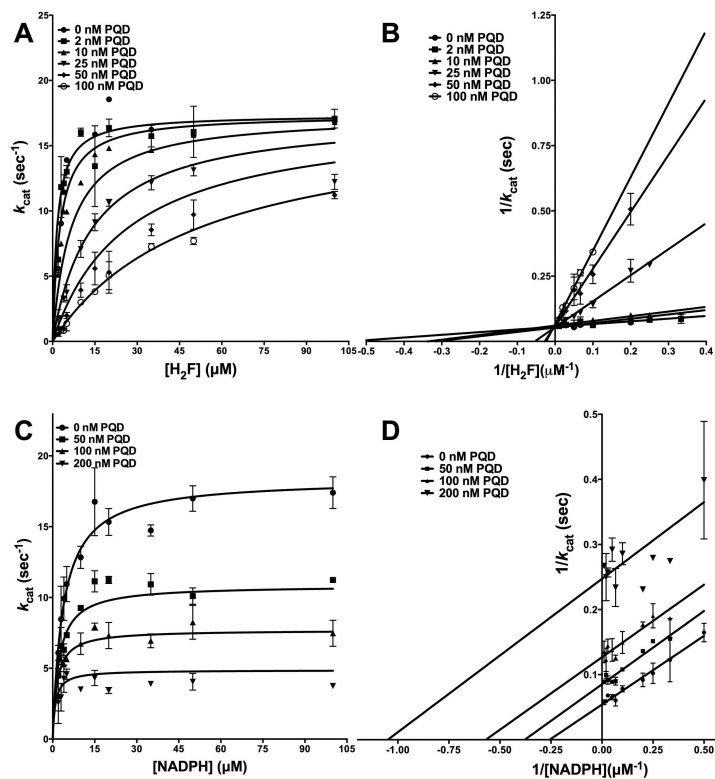


**Fig 5.** Inhibition kinetics of PQD (NSC339578) for *E. coli* DHFR (A) Fit of the primary data to the competitive inhibition model for H<sub>2</sub>F titration at several fixed concentrations of PQD. (B) Double reciprocal Lineweaver-Burk plot of H<sub>2</sub>F titration at several fixed concentrations of PQD. (C) Fit of the primary data to the uncompetitive inhibition model for NADPH titration at several fixed concentrations of PQD (D) Double reciprocal Lineweaver-Burk plot of NADPH titration at several fixed concentrations of PQD. The y-axis shows the  $k_{\text{cat}}$  value. The experimental data points were fit to the respective models using the non-linear curve-fitting algorithm of GraphPad Prism v 6.0e.

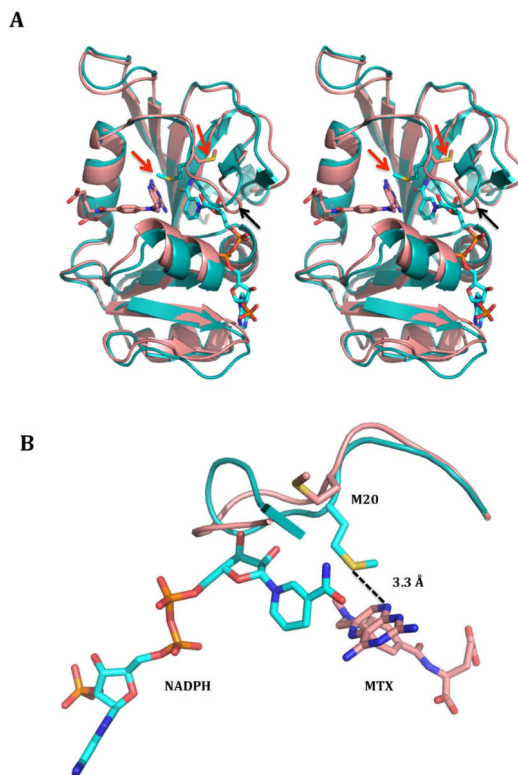


**Fig 6.** (A) Stereo image of the superimposed cartoon representation for NADPH-bound (PDB ID: 1RX1) and methotrexate-bound (PDB ID: 3DRC) *E. coli* DHFR highlighting the movement of M20 loop. The NADPH-bound structure is shown in teal color, the methotrexate-bound structure is shown in salmon color, and the ligands are shown in a stick representation in the respective colors. The red arrows indicate the position of the flipped methionine 20 and the black arrows show the movement of M20 loop upon NADPH binding. (B) Zoomed in representation highlighting the almost 180° flip of the methionine side chain in NADPH-bound *E. coli* DHFR that brings the thio group of methionine within hydrogen bonding distance of the N8 group of methotrexate. The hydrogen bonds are shown in dotted representation. The figures were generated with MacPyMOL.

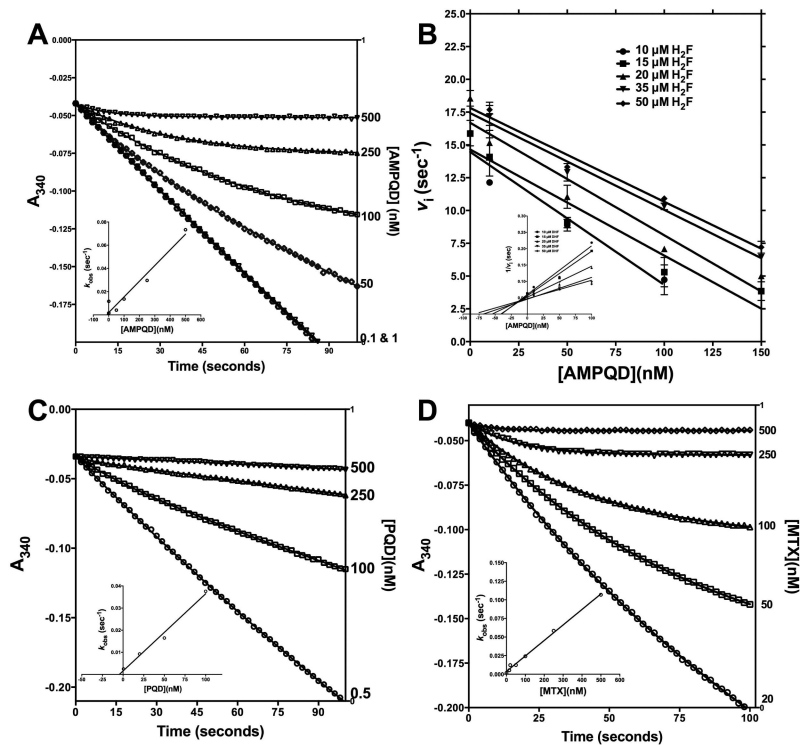


**Fig 7.** (A) Time-dependent inactivation of *E. coli* DHFR by 0–500 nM AMPQD. Inset shows the  $k_{\text{obs}}$  plotted as a function of [AMPQD] (B) Direct plot for the effect of AMPQD on the initial velocity of  $\text{H}_2\text{F}$  reduction of DHFR at various substrate concentrations. Inset shows the linearized plot of the data in (B). (C) Time-dependent inactivation of *E. coli* DHFR by 0–500 nM PQD. Inset shows the  $k_{\text{obs}}$  plotted as a function of [PQD] (D) Time-dependent inactivation of *E. coli* DHFR by 0–500 nM MTX. Inset shows the  $k_{\text{obs}}$  plotted as a function of [MTX]. The solid curves represent the best fit of the data to Eq. 7 for slow binding inhibition using of GraphPad Prism v 6.0e.

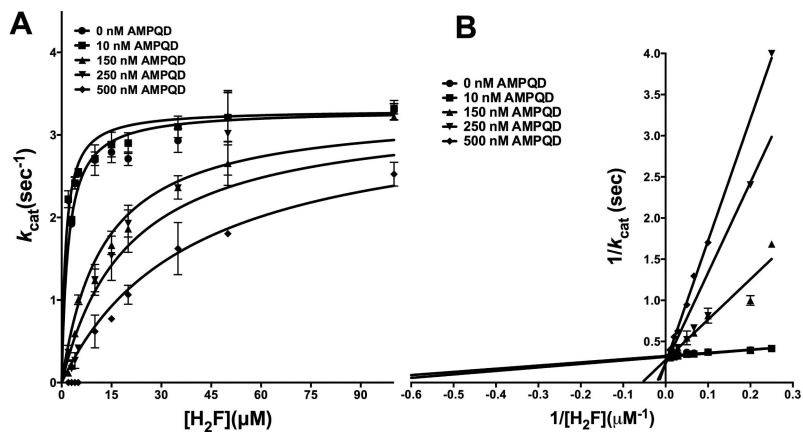


**Fig 8.** Inhibition kinetics of AMPQD (NSC309401) for human DHFR (A) Fit of the primary data to the competitive inhibition model for H<sub>2</sub>F titration at several fixed concentrations of AMPQD. (B) Double reciprocal Lineweaver-Burk plot of H<sub>2</sub>F titration at several fixed concentrations of AMPQD. The y-axis shows the  $k_{cat}$  value. The experimental data points were fit to the model using the non-linear curve-fitting algorithm of GraphPad Prism v 6.0e.

**Table 1**IC-50 and  $K_{iapp}$  values for various small molecule inhibitors of *E. coli* and human DHFR

Small molecule <sup>§</sup> / NSC ID	<i>E. coli</i> DHFR		Human DHFR	
	IC-50 (nM)	$K_{iapp}$ <sup>*</sup> (nM)	IC-50 (nM)	$K_{iapp}$ <sup>*</sup> (nM)
AMPQD/NSC309401	189.0 ± 1.0	7.8 ± 0.8	599.0 ± 7.2	19.4 ± 2.7
PQD <sup>#</sup> /NSC339578	106.1 ± 1.2	4.2 ± 0.5	3087.1 ± 16.5	93.4 ± 9.0
MTX <sup>#</sup> /NSC740	152.5 ± 1.1	6.7 ± 0.7	147.7 ± 2.3	5.1 ± 1.0
NNCPPU/NSC80735	36560 ± 1100	2062 ± 378	68870 ± 1356	1973 ± 329
NNBABD/NSC55152	176500 ± 1114	10941 ± 2156	254500 ± 1789	5161 ± 1411
ISB/NSC123458	587800 ± 1184	35222 ± 5358	ND	ND

\*  $K_{iapp}$  was estimated by employing the Morrison equation. This equation accounts for tight binding, and hence does not assume that the free concentration of inhibitor equals the total concentration.

# Reported inhibitors of DHFR from various organisms independently identified by our method as inhibitors of human and *E. coli* DHFR.

§ AMPQD, 7-[(4-aminophenyl)methyl]-7HPyrrolo[3,2-f]quinazoline-1,3-diamine; PQD, 7H-Pyrrolo(3,2-f)quinazoline-1,3-diamine; MTX, Methotrexate; NNCPPU, 1-(4-nitrophenyl)-3-[4-[4-(4-nitrophenyl) carbamoylamino] phenoxy]phenyl]urea; NNBABD, N,N'-bis(4-aminophenyl)benzene-1,4-dicarboxamide; ISB, 2,2'-Iminostilbene. ND, Not determined since it was greater than 2 mM.



**Table 2**Parameters from inhibition kinetics and time-dependent inactivation of *E. coli* DHFR

Inhibitors	Substrate	Inhibition #	$K_i/\alpha K_i$ (nM) *	$k_{off}$ (min <sup>-1</sup> )	$k_{on}$ (nM <sup>-1</sup> min <sup>-1</sup> )	$K_D$ (nM)
AMPQD	H <sub>2</sub> F	C	7.42 ± 0.92	0.118 ± 0.017	0.008 ± 0.001	14.57 ± 2.10
	NADPH	U	162.70 ± 9.06	NA	NA	NA
PQD	H <sub>2</sub> F	C	3.18 ± 0.51	0.094 ± 0.010	0.021 ± 0.002	4.48 ± 0.63
	NADPH	U	72.17 ± 4.23	NA	NA	NA
MTX	H <sub>2</sub> F	C	3.6 <sup>£</sup>	0.223 ± 0.078	0.013 ± 0.004	17.15 ± 2.92
	NADPH	U	111.00 ± 7.32	NA	NA	NA

# C: competitive inhibition, U: uncompetitive inhibition

\* The  $K_i$  reported is for competitive inhibition while  $\alpha K_i$  is reported for uncompetitive inhibition;  $K_D$  represents  $k_{off}/k_{on}$ ; NA, Not applicable.

£ The value reported is from the study [21]